

## Article

# Research on the Improvement of Granite Residual Soil Caused by Fly Ash and Its Slope Stability under Rainfall Conditions

Bowen Hu <sup>1</sup>, Qizhi Hu <sup>1,2,\*</sup>, Yiming Liu <sup>1</sup> and Gaoliang Tao <sup>1,2</sup> 

<sup>1</sup> School of Civil Architecture and Environment, Hubei University of Technology, Wuhan 430068, China; 102110877@hbut.edu.cn (B.H.); ymliu@hbut.edu.cn (Y.L.); tgl1979@126.com (G.T.)

<sup>2</sup> Hubei Bridge Safety Monitoring Technology and Equipment Technology Engineering Research Center, Wuhan 430068, China

\* Correspondence: hqz0716@163.com

**Abstract:** Granite residual soil has distinctive engineering characteristics due to its unique properties, and the resulting slopes are less stable and less resistant to rain erosion. The granite residual soil was improved by the addition of 5%, 10%, 15% and 20% fly ash, and the effects of fly ash on the intensity index and penetration of granite residual soil were investigated by triaxial strength tests and permeability tests. In combination with scanning electron microscopy measurements, a study of the stability of fly ash-modified granite residual soil slopes by modeling rainfall using the finite element software ABAQUS revealed the following: (1) the permeability coefficients of the residual granitic soils decreased by one order of magnitude when fly ash was added; (2) the improvement in the triaxial strength index of the improved soil was most pronounced when the dosage of fly ash was 15%, so that a dosage of 15% was considered optimal; and (3) numerical simulations concluded that the stability of the slope formed by 15% fly ash-improved soil fill improved significantly relative to the original slope, with the coefficient of safety increasing from 1.06 to 1.42, and the resistance to water seepage also significantly improved.

**Keywords:** granite residual soil; fly ash; triaxial shear test; permeability coefficient; slope stability



**Citation:** Hu, B.; Hu, Q.; Liu, Y.; Tao, G. Research on the Improvement of Granite Residual Soil Caused by Fly Ash and Its Slope Stability under Rainfall Conditions. *Appl. Sci.* **2024**, *14*, 3734. <https://doi.org/10.3390/app14093734>

Academic Editor: Suchao Xie

Received: 29 March 2024

Revised: 24 April 2024

Accepted: 26 April 2024

Published: 27 April 2024



**Copyright:** © 2024 by the authors. Licensee MDPI, Basel, Switzerland. This article is an open access article distributed under the terms and conditions of the Creative Commons Attribution (CC BY) license (<https://creativecommons.org/licenses/by/4.0/>).

## 1. Introduction

Granite residual soil is a special soil with favorable structural properties that is widely distributed in southeastern China and is a common soil in southern coastal areas [1]. Granite residual soil is easily disturbed, losing structural strength and easily disintegrating in contact with water [2], which leads to multiple engineering problems, such as slope instability and foundation collapse. Numerous researchers have studied the mechanical and hydraulic properties and slope aspects of granite residual soils. Yin et al. [3] studied the pattern of the microstructural evolution of granite residual soils in Shenzhen and found a phenomenon similar to overconsolidation in granite residual soils. Rahardjo H et al. [4] determined the foundation-bearing capacity of granite residual soils based on static load tests, side compression tests and indoor micro load tests based on the available information. Coutinho et al. [5] conducted field tests and indoor experiments on granite residual soils and found that slope destabilization in granite residual soils is mainly induced by rainfall. Zheng et al. [6] analyzed the reliability of granite residual soil slopes in Fujian and concluded that the slope reliability is related to the coefficient of variation and correlation of its soil parameters, and an instability may occur even when the slopes are considered to be stable based on the traditional factor of safety method. Using energy-dispersive spectroscopy, computer tomography, stereomicroscopy and scanning electron microscopy (SEM), Liu et al. [7] discovered a relationship between the horizontal fissure and the strength anisotropy of the material. Gomes et al. [8] proposed the use of pressure plates and filter paper methods to determine the water–soil characteristic curve (SWCC) for granitic residual soils, corrected several equations based on the experimental data and

discussed the results. A database of 237 small strain stiffness measurements made on 35 distinct residual soils by G. Veylon et al. [9] is given. The characteristics determining the way saturated residual soils react to tiny strains are discovered and recommended based on a thorough and well-justified investigation.

The protoliths of granite residual soil are composed mainly of quartz, mica, hornblende, feldspar and other fine-grained materials [10]. The chemical weathering process of granite is dominated by the reaction of feldspar, which accounts for the largest proportion, with an aqueous solution, water, oxygen and carbon dioxide forming kaolinite, the content of which increases with the degree of weathering; kaolinite is hydrophilic and softens with water under dry conditions [11,12]. The southern region of China has a tropical and subtropical monsoon climate, and due to abundant rainfall in the summer, a large amount of heavy rainfall leads to the occurrence of avalanche erosion and soil erosion in the region [13], of which the runoff erosion phenomenon is more important in Jiangxi Province. Under the influence of rainfall infiltration, because of the soil shear resistance of the slopes formed by granitic residual soils, the shear strength of the slopes formed by residual soils is greatly reduced, and construction accidents such as slips and landslides increase the risk of destabilizing engineering accidents in the absence of protective measures [14]. Therefore, for effective engineering, it is important to improve the soil properties of granite residual soil slopes.

To address the undesirable nature of granite residual soils that soften and disintegrate in the presence of water, they are usually improved and reinforced with soil-curing agents, including lime [15,16], lignin [17], fly ash [18] and cement [19]. Among these, fly ash is a coal byproduct produced in the combustion of coal in power plants, with high emissions, which can cause air pollution and other ecological and environmental problems. Therefore, many researchers have investigated the possible applications of fly ash [20–22]. Several researchers have explored the reinforcing effect of fly ash on soils via indoor tests. Li et al. [23] utilized fly ash to improve sandy soil and found that the incorporation of fly ash into sandy soil can effectively improve the shell capacity of sandy soil. Liu et al. [24] mixed granite residual soil and fly ash and found that fly ash effectively enhanced the shell capacity of granite residual soil after treatment. Through conventional indoor tests, microanalysis and other means, Xie et al. [25] concluded that fly ash particles improve granite residual soil by occupying large pores in the ground, which gives rise to mutual adhesion. These studies have shown that fly ash can enhance the intensity of granite residual soils.

Some researchers have investigated the durability of granite residual soil slopes in engineering applications after rainfall. The disintegrability of granite residual soil slopes and the breakdown of their internal structure were examined by Wang et al. [26]. The rainfall seepage path of granite residual soil side slopes was numerically simulated by Li et al. [27] under conditions of precipitation infiltration. The impact of rainfall on the internal deformation characteristics of granite residual soil slopes and slope-destabilizing processes was simulated by Xu et al. [28]. The damage pattern in granite residual soil slope landslides during rainfall circumstances, as well as the correlation between slope landslides and rainfall intensity, were investigated by Hu et al. [29]. Guo et al. [30] investigated the course of rainfall penetration in granite residual soil road-graben slopes and found that rainwater infiltration altered the original stable state of the slopes. Chen et al. [31] conducted an indoor modeling experiment on the hydrological impacts of granite residual soil slopes under artificial precipitation considering three vegetation types. For granite residual soil slopes, Xu et al. [32] created a gray cusp catastrophic destabilization forecasting system that can calculate the destabilization period of granite residual soil slopes under rainfall circumstances. The impact of slope angle on the slope instability during intense rainfall avalanche erosion of residual soil slopes was investigated by Liu et al. [33]. A study on the impact of the grain diameter composition of granite residual soil on rainfall slopes was started by Liu et al. [34]. Using the physical models that Yang et al. [35] used, field monitoring data are crucial for the back analysis of soil characteristics and offer important insights into the mechanisms underlying granite residual soil slope instability.

These findings revealed that fly ash improves the pore structure. It can also increase the strength of soils, including granite residual soils. Much of the reported research has focused on the physical properties of fly ash-amended soils, while the rainfall erosion resistance and stability of fly ash applied to slope protection under rainfall conditions still need to be investigated further. Therefore, fly ash was chosen as an improvement treatment for the granite residual soil on a slope of a segment of a highway from Anyuan County to Dingnan County. The undrained triaxial consolidation test and the variable head infiltration test were performed to examine the shear strength and permeability changes of the improved granite residual soil, and SEM measurements were used to examine the mechanism of fly ash reinforcement of the granite residual soil from a microscopic perspective. Additionally, the fly ash-improved soil dosage and strength of a backfilled slope after heavy rainfall were simulated using the finite element method. Furthermore, the improvement of granite residual soil slopes under rainfall conditions due to the addition of fly ash to the soil was analyzed. The main purpose of this study is to realize the application of fly ash in the protection of granite residual soil slopes, to solve the problem of environmental pollution caused by a large amount of accumulated fly ash and to provide a reference basis for the disaster of granite residual soil landslides caused by similar terrain and rainfall conditions.

## 2. Test Materials and Test Methods

### 2.1. Test Materials

The test soil was collected from a location in Ganzhou City, Jiangxi Province, as shown in Figure 1; it is a typical granite residual soil, with yellowish brown, grayish white and various hues mixed in with white dots. Following its retrieval, the granite residual soil was air-dried in the laboratory behind a shade structure, crushed using a wooden stick on a rubber mat and sieved to remove coarse particles with sizes larger than 2 mm. The geotechnical test procedures were followed in compliance with the fundamental physical characteristics of the soil sample test. The drying method was used to measure the soil samples' moisture content, the ring knife method was used to measure the soil's natural density, a combined liquid-plastic limit apparatus was used to determine the soil samples' liquid-plastic limit, the lightweight compaction test was used to determine the soil samples' optimal moisture content and the maximum dry density of the soil samples was calculated. Table 1 displays the physical indices of the soil. Fly ash was purchased from Henan Platinum Run Foundry Materials Co., Ltd., a company located in Henan Province, China, and its material composition data comes from this company. The material composition properties of the fly ash are shown in Table 2 and Figure 2. The material composition of the fly ash is in the range of common fly ash material compositions [36–38].



Figure 1. Granite residual soil.

**Table 1.** Physical properties of granite residual soils.

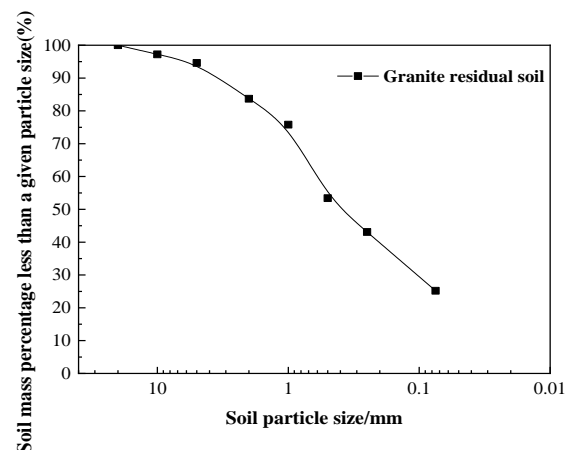
Natural Moisture Content/%	Natural Density/(g/cm <sup>-3</sup> )	Liquid Limit/%	Plastic Limit/%	Maximum Dry Density/(g/cm <sup>-3</sup> )	Optimum Moisture Content/%	Porosity Ratio
24.5	1.93	40.59	24.41	1.614	21.34	0.802

**Table 2.** Chemical composition of the fly ash (%).

SiO <sub>2</sub>	Al <sub>2</sub> O <sub>3</sub>	Fe <sub>2</sub> O <sub>3</sub>	CaO	MgO	Na <sub>2</sub> O	Other Ingredient Content
49.1	29.2	7.4	5.6	2.5	3.4	2.8

**Figure 2.** Fly ash.

The soil samples were simply sorted to eliminate the few larger particles to limit the dispersion of the test results. Then, sieving tests were conducted to produce the particle-grading curves of the granite residual soil used for the test, as shown in Figure 3.

**Figure 3.** Particle-grading curves of soils.

Fly ash was combined with granite residual soil to examine the beneficial effects of fly ash on the soil. Mixed soil samples with fly ash dosages (mass ratios) of 5%, 10%, 15% and 20% were obtained. The light compaction test was used to determine the maximum dry density and ideal water content of the mixed soil samples with varying fly ash contents. The test results are displayed in Table 3.

**Table 3.** Physical indices of granite residual soil with different fly ash concentrations.

Fly Ash Dosage	Maximum Dry Density/(g/cm <sup>-3</sup> )	Optimum Moisture Content/%
5	1.642	20.96
10	1.657	19.33
15	1.671	19.20
20	1.704	18.87

The prepared specimens were subjected to ordinary triaxial tests and variable head infiltration tests as well as corresponding data analysis according to the Standard for Geotechnical Test Methods (GB/T 50123-2019), and the specimens with the best test results in each group were selected for SEM scanning to determine the mechanism of strength growth and infiltration change in the granite residual soils improved by fly ash.

## 2.2. Test Methods

### 2.2.1. Triaxial Test

The Nanjing Soil Instrument Factory TSZ-2 strain control instrument, which is a fully automatic triaxial instrument, was used for the tests, and the test apparatus is shown in Figure 4. This instrument is from Jiangsu Province, China. The granite residual soil with different contents of fly ash was mixed according to the geotechnical test procedure, cylindrical specimens of  $\Phi 39.1 \text{ mm} \times 80 \text{ mm}$  were obtained by layered compaction, with fifteen specimens obtained from five groups of three specimens each, with fly ash contents of 0%, 5%, 10%, 15% and 20%. To achieve sufficient strength, cylindrical specimens were fabricated and then cured for 14 d at  $25 \text{ }^\circ\text{C}$  and  $90 \pm 2\%$  humidity in a curing box. This ensured that the fly ash was thoroughly mixed with the granite residual soil. Then, the specimen was soaked using vacuum pumping in preparation for the triaxial test. A prepared specimen is displayed in Figure 5. The accuracy of the test was ensured by averaging two parallel tests.



**Figure 4.** TSZ-2 fully automatic triaxial test system.



**Figure 5.** Specimen of granite residual soil amended with fly ash.

Using a triaxial instrument, a solidification undrained shear test was performed. The peripheral pressure was 100, 200 and 300 kPa, and the shear rate was fixed at 0.01 mm/min.

Because the test was strain-controlled, the specimen was deemed to have been sheared when its axial strain reached 20%.

### 2.2.2. Penetration Tests

A variable head infiltration test was used to measure the infiltration coefficient of granite residual soil with different fly ash admixtures. The Nanjing Ningxi Soil Instrument Factory TST-55, infiltrometer was used for the test, and the infiltration test apparatus is shown in Figure 6. This instrument is from Jiangsu Province, China. A ring knife with  $\Phi 61.8 \text{ mm} \times 40 \text{ mm}$  was used to obtain the sample prepared by the pressure sample method. Five kinds of specimens with fly ash contents of 0%, 5%, 10%, 15% and 20% were prepared. The permeation test was carried out after the specimens were prepared and cured for 14 d in a curing box at a temperature of  $25 \text{ }^\circ\text{C}$  and humidity of  $90 \pm 2\%$ . The permeability coefficient  $K$  of the specimen was calculated after the completion of the permeability test according to the following equation:

$$K = 2.3 \frac{aL}{A(t_1 - t_2)} \lg \frac{H_1}{H_2} \quad (1)$$

where  $K$  is the coefficient of permeability (cm/s);  $t_1$  and  $t_2$  are the start and termination times of the head reading (s);  $H_1$  and  $H_2$  are the start and termination times of the height of the water head (m), respectively;  $a$  is the cross-sectional area of the variable head pipe ( $\text{cm}^2$ );  $A$  is the cross-sectional area of the specimen ( $\text{cm}^2$ ); and  $L$  is the seepage diameter or the height of the specimen (cm).



Figure 6. TST-55 penetrometer.

## 3. Test Results and Analysis

### 3.1. Triaxial Shear Test Results and Analysis

#### 3.1.1. Stress–Strain Relationships

Figures 7–11 display the stress–strain curves of the modified soil and granite residual soil plain under various enclosing pressures. As shown in Figure 6, the bias stress exhibits a transient linear increase at axial strain  $\varepsilon < 2\%$ , followed by a nonlinear increase, and the stress–strain curve of the plain soil is of the strain-hardening type. Figures 7–10 show that the curve of the enhanced soil with the fly ash admixture displays a strain-softening type, meaning that the specimen's stress first increases with strain and then stops increasing when the strain reaches a particular amount. Following an increase in the perimeter pressure, the axial stresses at the damage of the four doped fly ash-amended soils increased concurrently. The axial stresses of the four doped fly ash-amended soils simultaneously increased upon damage when the perimeter pressure increased from 100 kPa to 300 kPa. A comparison of the stress–strain curves of the two soil samples shows that the soil treated with fly ash had better structural characteristics than the plain soil. The peak strengths of the vegetative soil for each of the perimeter pressures are lower than the peak strengths of

the fly ash-modified soil at the same perimeter pressure, assuming that the bias stress at 20% strain is the peak strength.

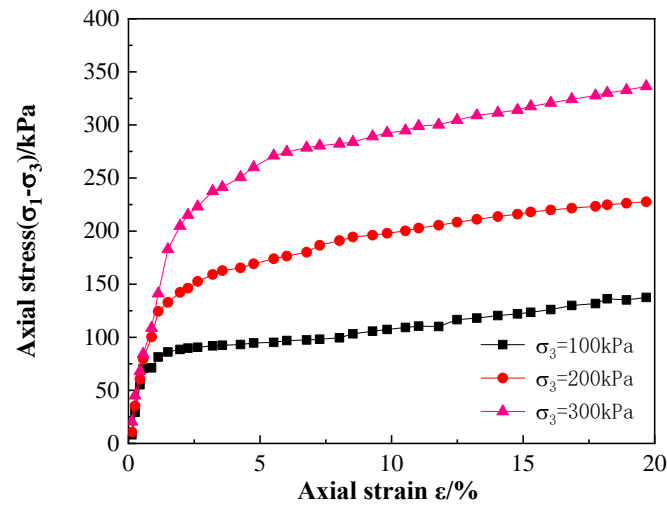


Figure 7. Stress-strain curves of the plain soil.

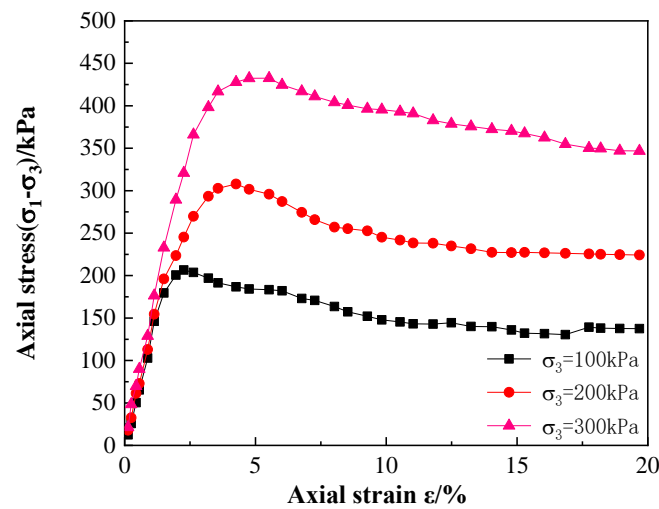


Figure 8. Stress-strain curves of the modified soil with 5% fly ash.

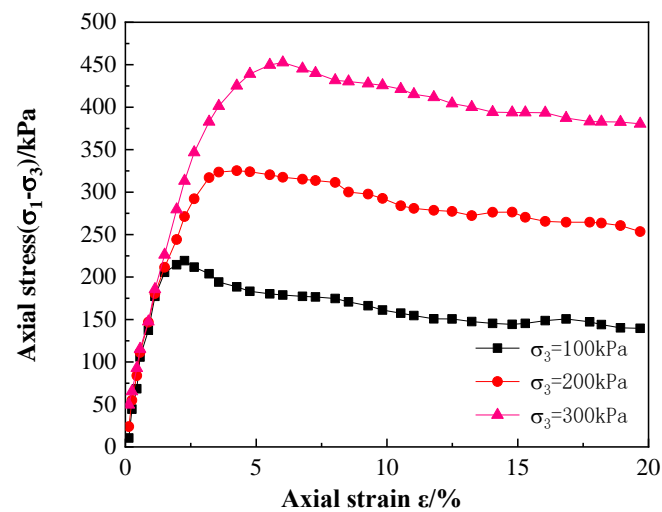


Figure 9. Stress-strain curves of the modified soil with 10% fly ash.

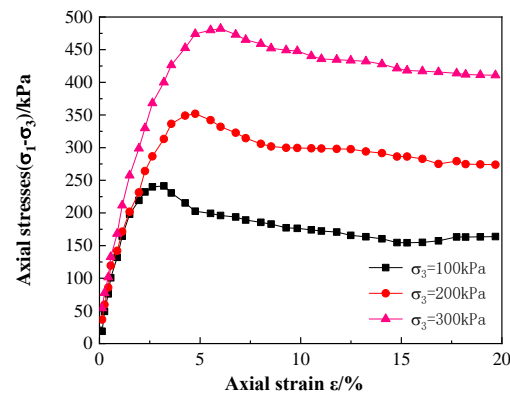


Figure 10. Stress-strain curves of the modified soil with 15% fly ash.

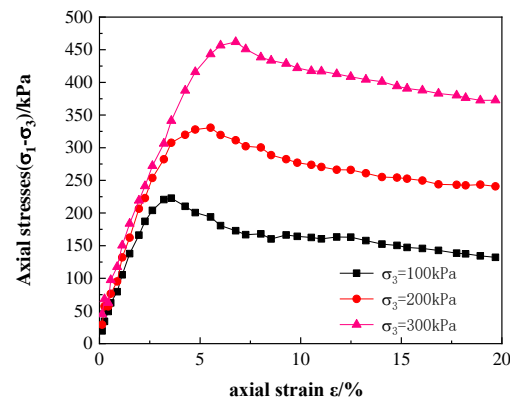
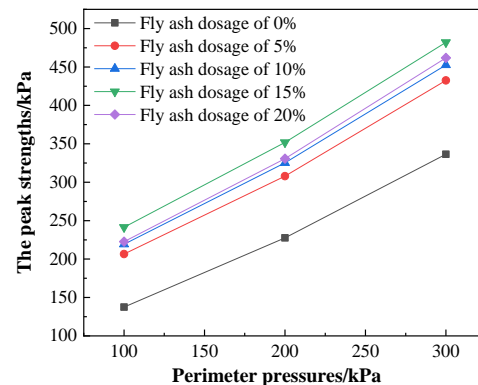


Figure 11. Stress-strain curves of the modified soil with 20% fly ash.

The variation curves of the peak strengths of the soils modified with pulverized coal and five fly ash admixtures at varying enclosure pressures are displayed in Figure 12. The peak strength of each doped soil body is strongly associated with the perimeter pressure, as shown in Figure 12. At the perimeter pressures of 100, 200 and 300 kPa, the peak strengths of the fly ash-amended soil specimens modified with 5% fly ash increased by 50.21%, 36.17% and 28.56%, respectively, in comparison to those of the plain soil specimens. The peak strengths of the fly ash-modified soil specimens with 10% admixture increased by 42.90%, 34.54% and 59.41%, respectively, in comparison to those of the plain soil specimens; these increases were 75.54%, 54.59% and 43.30%, respectively, for the soil specimens modified with 15% fly ash and 61.88%, 45.30% and 37.29%, respectively, for the soil specimens modified with 20% fly ash. Compared with those of the plain soil specimen, the soil specimens modified with 20% fly ash showed peak strength increases of 61.88%, 45.30% and 37.29%. The specimens' peak stress first increases as the fly ash dosage increases from 0% to 15%, and then decreases as the fly ash dosage increases to 20%. This indicates that there is an optimal dosage value of 15% for enhancing the strength of the granite residual soil with fly ash. The significant internal porosity, relatively loose soil skeleton and poorly connected soil particles in the granite residual soil give rise to this trend. The tiny particles of the material fill the pores in the granite residual soil once the fly ash is added. The silica and alumina in the fly ash also experience a hard coagulation reaction with the granite residual soil, enhancing the coagulation ability of the soil. Furthermore, when fly ash and water come into contact, the fly ash can initiate a hydration reaction that results in the formation of a gelling material that reinforces the soil body and further bonds the soil particles. When the fly ash dose was increased from 0% to 15%, the fly ash particles adhered to the granite residual soil more firmly, and the strength of the granite residual soil increased concurrently. The reinforcing effect of fly ash on the soil is weakened when the dosage is increased to 20% because the fly ash particles essentially fill the pores in the granite residual soil, and the excess fly ash particles are not present in the soil, reducing

the size of the soil skeleton. Although the strength of the soil is still greater than that of vegetative soil, the impact is not as great as that of a 15% addition of fly ash to the soil.



**Figure 12.** Variation in the peak strength as a function of the peripheral pressure.

### 3.1.2. Strength Characterization

Moore's stress circle was drawn on the right-angle coordinate system based on the relationship between the axial strain and bias stress. The effective stress–shear strength expression and the effective stress strength indices (angle of internal friction and cohesion) of the specimens with different fly ash admixtures were calculated to obtain the effective shear strength indices of the granite residual soil with different fly ash admixtures. The results are displayed in Figure 13.

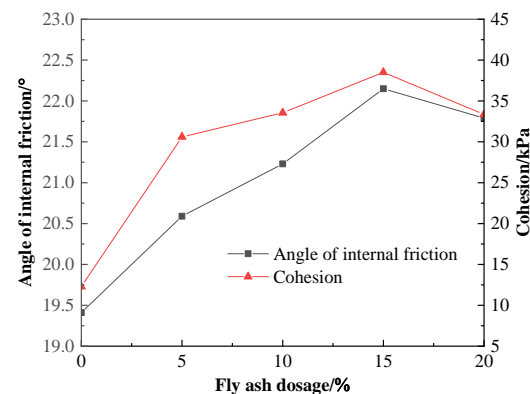


**Figure 13.** Variation of the effective cohesion and effective internal friction angle of granite residual soil specimens with different fly ash contents.

Fly ash was added, and as shown in Figure 13, this greatly increased the shear strength index of the granite residual soil. Their cohesiveness and angle of internal friction of the fly ash-modified granite residual soil first increased and then decreased. The effective cohesion of the vegetative soil was measured as 12.28 kPa, and its internal friction angle was 19.41°. The highest shear strength index was found in granite residual soil treated with 15% fly ash, with an internal friction angle of 22.15° and effective cohesion of 38.51 kPa. In comparison to vegetative soils, all four types of fly ash-amended soils showed enhanced cohesion and a greater angle of internal friction. This is because the fly ash and water combined to form a gelling substance. As the fly ash content increased, the lubricating effect gradually diminished, and the ability of the water film to bind the particles together weakened, increasing the friction between the soil particles and the granite residual soil angle of internal friction. When combined with fly ash, this gelling material closes the soil's internal pores, decreases the soil porosity, increases the soil compactness and strengthens the bonds between the soil particles. However, after the dosage of fly ash reaches 20%, excess fly ash appears, which reduces the internal skeleton of the soil body, resulting in

reduced friction between the soil particles and weaker adhesion between the soil particles, thus reducing the angle of internal friction and cohesion.

### 3.2. Changes in Permeability

The curves of the permeability coefficient plotted versus the fly ash dosage variation are displayed in Figure 14. The permeability coefficient of the plain soil is  $5.29 \times 10^{-5}$  cm/s, while the permeability coefficients of the granite residual soil with fly ash dosages of 5%, 10%, 15% and 20% are  $6.68 \times 10^{-6}$ ,  $6.92 \times 10^{-6}$ ,  $7.13 \times 10^{-6}$  and  $6.83 \times 10^{-6}$  cm/s, respectively. As shown in Figure 14, the permeability coefficient of the improved soil mixed with fly ash decreases by an order of magnitude. The permeability coefficients of the improved soils with different fly ash dosages do not differ significantly, and the permeability coefficient of the granite residual soil cannot be significantly decreased by adding more fly ash to the mixture. According to the results obtained by Zhang [38], CaO in fly ash reacts with water to produce  $\text{Ca(OH)}_2$ , while  $\text{SiO}_2$  and  $\text{Al}_2\text{O}_3$  in fly ash react with  $\text{Ca(OH)}_2$  to produce gelling substances such as calcium aluminum and calcium silicate minerals, reducing the effective pore space of granite residual soil. The permeability coefficient of granite residual soil decreases due to the cementitious materials and fly ash filling the pore space in the soil, leading to some improvement in the resistance of the soil to rainwater erosion. Notably, when the fly ash dose was changed from 5% to 20%, the enhanced soil permeability coefficients increased. This may be because the optimal water content is greater when the fly ash dosage is 5% compared to other fly ash dosages of improved soil, and when the reaction between fly ash and granite residual soil occurs, a sufficient amount of water is available around the fly ash particles, leading to a more sufficient reaction compared to the other dosages of improved soil; therefore, a lower permeability coefficient is obtained.

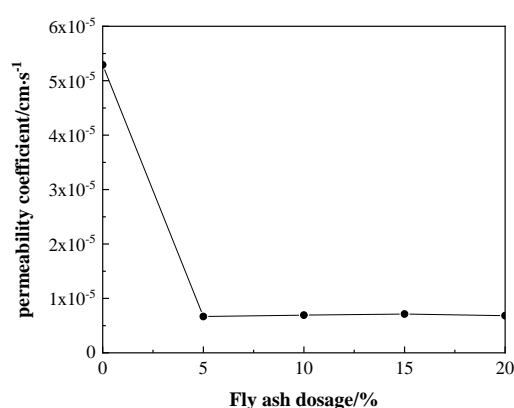


**Figure 14.** Relationship of the permeability coefficient with fly ash dose.

### 3.3. Improved Mechanisms

SEM tests were carried out on granite residual soil amended with fly ash at 0%-20% admixture. The gold-spraying treatment instrument was an SBC-12 ion sputtering instrument from Langfang Zhongyi Technology Co., which located in Hebei Province, China, and the soil section was tested using a JSM-7800F field emission scanning electron microscope from Japan Electron Optical Laboratory.

Figure 15 shows the SEM images of the granite residual soil at  $500\times$  and  $2000\times$ . As observed from the  $500\times$  image, granite residual soil particles are represented by the areas in the picture with high brightness and light color, while granite residual soil pores are represented by the areas with low brightness and dark color. The image illustrates how the vegetal soil particles are loosely skeletal and unevenly massive. Fly ash particles are shown by the round, spherical material in the picture. The SEM image of the modified soil clearly shows the presence of fly ash particles, which are clearly visible and dispersed throughout the soil interstitials inside the fly ash-doped soil samples. With fewer and more dispersed fly ash particles, the fly ash-improved soil with 5% and 10% fly ash content

produces less cementitious material and has a higher porosity than fly ash dosages of 15% enhanced the soil. With a total of 15% fly ash in granite residual soil, fly ash particles plug soil pores and produce a gelatinous substance; the cementitious material indicated in the figure is easily observable, and the SEM diagrams show how part of the gelatinous substance is wrapped around the fly ash particles. The soil particles are bound together by fly ash particles and the gelatinous substance. A total of 20% of the dosed fly ash specimen in the fly ash particles was too much; this is evident from the image, which shows that some of the fly ash particles emerged in a condition of “aggregation,” meaning that they were not completely filled in the granite residual soil but rather were next to one another. In this condition, the structural qualities of the granite residual soil are diminished, and its net content also declines, weakening the soil body’s skeleton and strength.

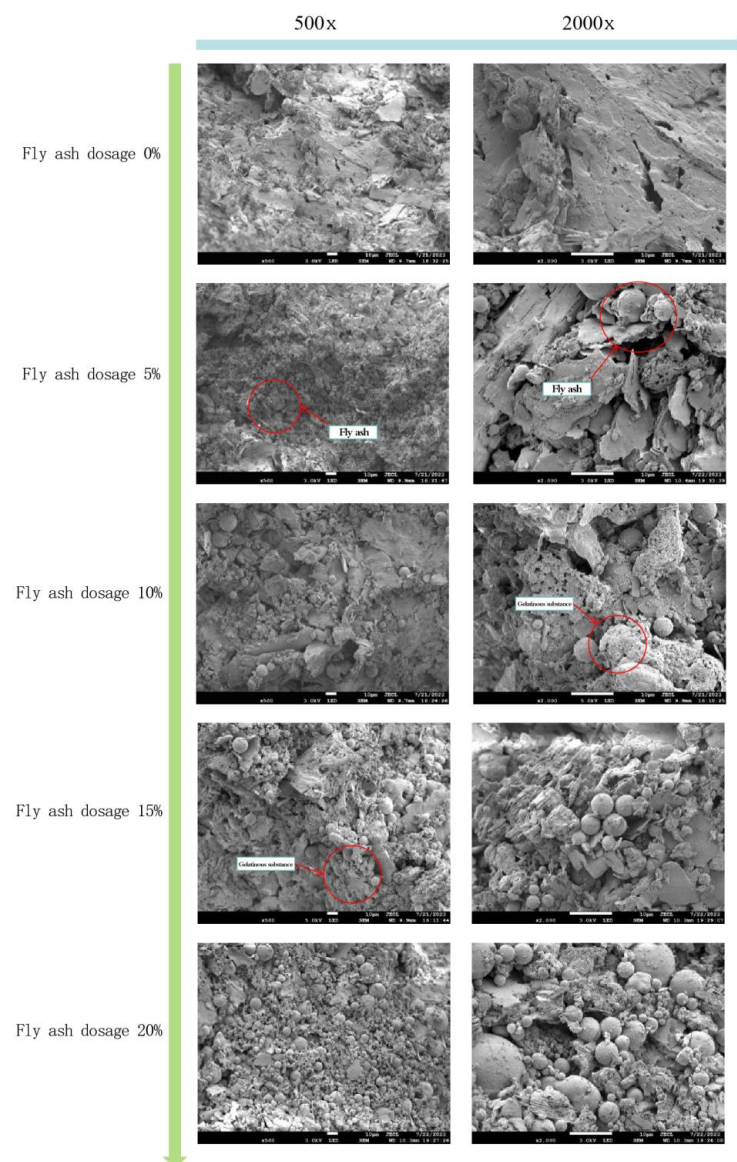


**Figure 15.** SEM images of granite residual soil with different fly ash dosages at 500 $\times$  and 2000 $\times$ .

From the 2000 $\times$  SEM image, it can be found that the surface of the plain soil specimen is smoother, flatter and more porous. There were visible fly ash particles in the pores of the enhanced granite residual soil mixed with fly ash, and the improved soil with fly ash dosages of 5% and 10% still had visible pores. Fly ash dosages of 15% and 20% enhanced the soil, clearly reduced the number of pores and mostly revealed fly ash particles and a gelatinous substance. The hydration process between the fly ash and the water adhering to

the surface of the soil particles, or partially enclosed in the fly ash, produces this gelling substance, which takes the form of a net or floc structure. The internal pores of the granite residual soil were plugged by the produced gelatinous substance and fly ash particles, creating a more tortuous hydraulic infiltration channel. This confirms the results of the infiltration test reported in the previous section, namely that the seepage resistance of granite residual soils can be successfully increased by the addition of fly ash.

#### 4. Engineering Applications

Ganzhou City, Jiangxi Province, with a longitudinal distance of 295 km and a horizontal distance of 219 km, has a total area of 39,379.64 square kilometers, accounting for 23.6% of the total area of Jiangxi Province, making it the largest administrative district in the province. In terms of geological composition, Ganzhou City has a wide distribution of granite, and thus a large amount of granite residual soil exists. The liaison line of the highway from Anyuan County to Dingnan County is a highway in Ganzhou city connecting Anyuan County and Dingnan County, and its side slopes consist of typical granite residual soil; a map of the study area is shown in Figure 16. The slope is a half-filled and half-excavated slope with a cross-sectional filling height of 11 m, slope width of 21.5 m and slope gradient of  $31\sim 33^\circ$ ; the model is schematically shown in Figure 17 [39]. The slope is used as an example for slope stability analysis.

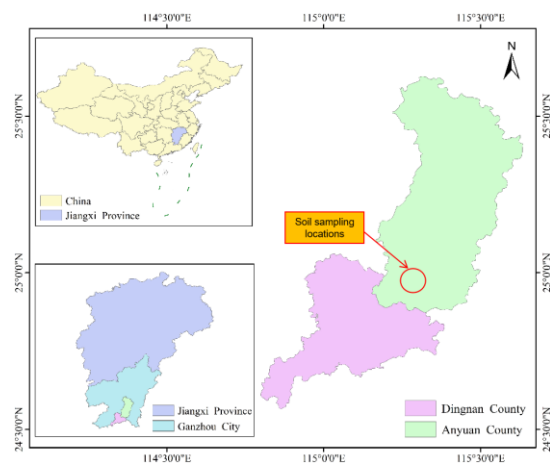


Figure 16. Location of the study area.

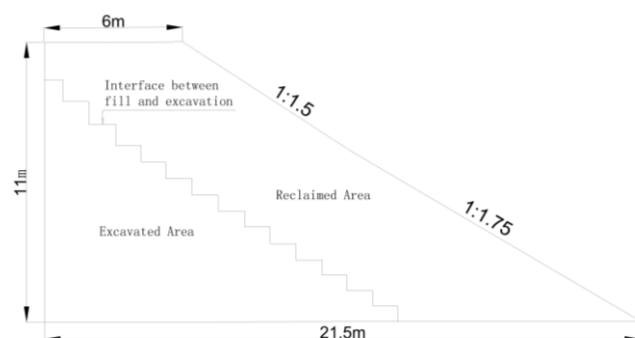


Figure 17. Schematic diagram of actual engineering slope modeling.

Numerical simulation of granite residual soil slopes was carried out using the ABAQUS finite element analysis software version 2022. ABAQUS is a powerful finite element simulation software used in engineering. Geotechnical engineering, involving seepage, flow–solid coupling analysis and other issues, is often a nonlinear problem, and ABAQUS can be used for the analysis of these issues to achieve better results. ABAQUS analyses can couple permeation and deformation problems by treating solid- and liquid-phase systems as an overlapping continuum and ignoring the microscopic shape of the porous medium [40].

Additionally, ABAQUS has a rich built-in soil instinctive model for high-quality simulation of the soil properties, displacement and stress during soil instability [41]. Therefore, ABAQUS is well-suited to solving geotechnical engineering problems, and results obtained using ABAQUS can be used as a guide for solving physical engineering problems.

For finite element modeling, the grid cells are turned on in hybridization mode and selected as eight-node quadrilaterals with reduced integral pore fluid cells, i.e., CPE8RPH cells, for a total of 11,313 cells. The boundary range of the model during finite element calculations will have some influence on the calculation accuracy, and the original slope size must be increased appropriately. Therefore, to ensure computational accuracy, the height of the model is taken to be two times the slope height, and the distance from the slope foot to the border is taken to be 1.5 times the slope height. The simulation mesh division is displayed in Figure 18. The backfill area of the slope model is configured with two sets of material parameters corresponding to plain soil and enhanced soil, based on the actual slope data. The Moore–Cullen primary model is used for both materials and the parameters are displayed in Table 4. The material parameters are derived from the data already measured in the previous chapter with the basic properties of granite residual soils. The following assumptions are made about the material: the material is homogeneous, continuous and isotropic.

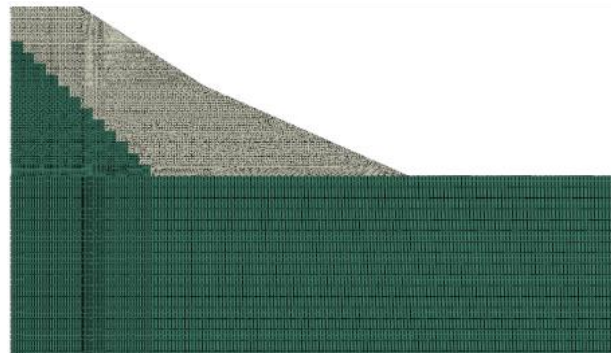


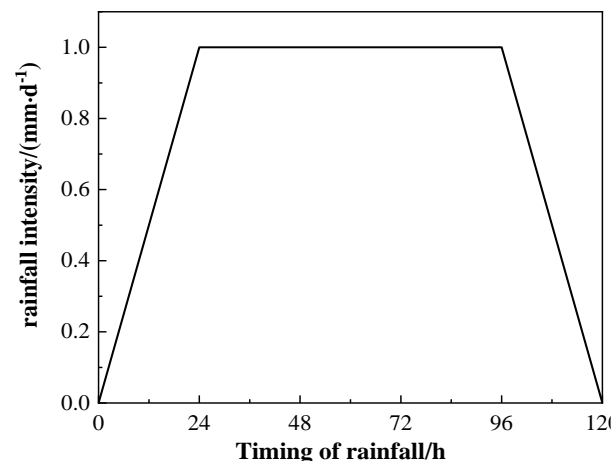
Figure 18. Slope calculation model.

Table 4. Physical and mechanical parameters of finite element model materials.

Materials	Cohesion/kPa	Angle of Internal Friction/°	Permeability Coefficient ( $\times 10^{-5}$ cm·s <sup>-1</sup> )	Poisson's Ratio	Modulus of Elasticity/MPa
Unimproved granite residual soil	12.28	19.41	5.29	0.3	5
Fly ash amended soil	38.51	22.15	0.71	0.3	5

#### 4.1. Rainfall Conditions

The study area has a humid subtropical monsoon climate, with average annual rainfall ranging from 1341.4 to 2259.6 mm and overall rainfall showing uneven spatial and temporal distributions and high extremes [42]. According to the rainfall statistics for the last five years of the Anyuan County to Dingnan County Expressway Project, it is found that heavy rainfall occurs frequently in the region, especially in certain months, which is particularly alarming, such as the rainfall in May 2015, which was as high as 570 mm. And from April to June every year, which is the rainy season in Gannan, the rainfall in these two seasons accounts for nearly 80% of the annual rainfall, showcasing the abundant rainfall in the region. According to the climatic conditions of the project site, the simulated rainfall was set to 50 mm/d. The simulated slopes started to receive rainfall at 0 h, and the change in the rainfall intensity gradually increased from 0 to 24 h and reached a maximum at 24 h; at 96–120 h, the rainfall intensity gradually decreased, and at 120 h, the rainfall intensity reached 0, corresponding to the end of the rainfall event. The curve of the change in the rainfall intensity of the slope model is shown in Figure 19.



**Figure 19.** Rainfall intensity versus time curve.

#### 4.2. Boundary Conditions

The horizontal constraints at the left and right ends of the model are given concurrently with the vertical restrictions at the bottom of the slope model. The real force conditions are taken into consideration when setting these model boundary criteria. To replicate the groundwater level distribution at the slope's base, the pore pressure between the soil and air contact surface on the right side of the slope's foot should be set to zero. Additionally, the pore pressure at other points increases linearly with increasing distance from the top surface of the soil layer outside the slope's foot, in accordance with the pore pressure distribution function, and Equation (2) is used to represent the pore pressure distribution function.

$$P = (11 - Y) \times 9.81 \quad (2)$$

where  $P$  is the pore pressure at a point in the model (kPa) and  $Y$  is the perpendicular distance of the point from the bottom boundary of the model (m), i.e., the vertical coordinate of the point in the model.

In practice, slope deformation is caused by the force of gravity when the slope is subjected to loading. However, in the simulations using finite element software, the initial state of the model is gravity-free and no stress exists, which can lead to a large deviation of the model calculations from the actual engineering situation. Therefore, when only one slope gravity is considered, the slope model must be calculated once, and the initial state in the subsequent calculations is the result after the first calculation.

#### 4.3. Finite Element Simulation

##### 4.3.1. Analysis of the Slope Displacement Results

Figures 20 and 21 show the total slope displacements of two different soil samples after 120 h of rainfall, at which time the material properties did not decrease, and the slope displacements were caused by the rainfall. Figure 20 shows that the total slope displacement decreases due to the incorporation of fly ash, and the maximum slope displacement remains at the junction of the filled area and the unexcavated surface. The total displacements of the plain soil slopes and fly ash-improved soil slopes were 8.35 cm and 1.42 cm, respectively, and the total displacements of the fly ash-improved slopes were reduced by 82.99% compared to those of the plain soil slopes. The maximum displacement of the granite residual soil backfilled with fly ash was greatly reduced, and the slope displacement changed from a shallow distribution concentrated in the filling area to a uniform distribution over the entire slope. That is, after fly ash improvement, the displacement of the granite residual soil slope under rainfall conditions is characterized by uniform settlement, which is conducive to slope stability.

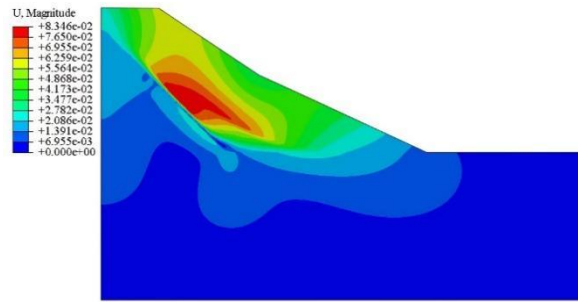


Figure 20. Displacement cloud of the vegetated soil slope.

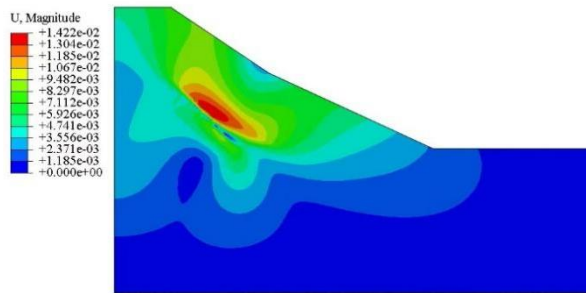


Figure 21. Displacement cloud of the modified soil slope.

#### 4.3.2. Characterization of the Distribution of Plastic Zones

The distribution map of the slope’s plastic zone and the corresponding effect variable, PEMAG, are vital in identifying whether a slope is destabilized. PEMAG, in particular, may characterize the plastic strain at a specific point in the slope deformation process. The distribution of plastic zones on the slopes was characterized using PEMAG maps of the slopes that received less than 120 h of rainfall. The plastic strain equivalent cloud plots of the two soil samples during a rainstorm are displayed in Figures 22 and 23. While the rainfall effect of the vegetative soil slope appeared to extend the foot of the excavation surface upward in the shape of a circular arc of the plastic zone, from the foot of the slope to the top of the longitudinal section of the slope, close to the sliding surface, Figure 22 demonstrates that the plastic zone of the improved soil slope extended to the inside of the slope, not forming a large area of the plastic zone through the slope. The comparable plastic strain on the improved soil slope was an order of magnitude lower than that of the plain soil, at 85.29%.

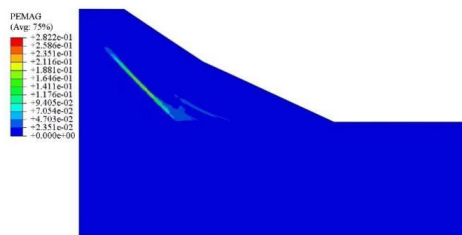


Figure 22. Cloud map of the plastic zone of a vegetative slope.

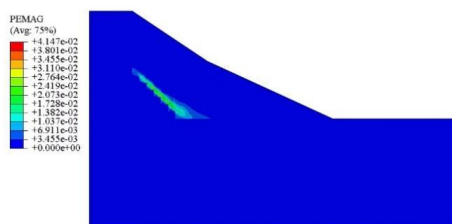


Figure 23. Cloud map of the plastic zone of a modified slope.

### 4.3.3. Slope Stability Analysis

There are three main criteria for discriminating slope instability with the strength discounting method, among which the slope displacement inflection point has a clear physical meaning and can be combined with slope displacement monitoring in practical engineering. The strength discounting method in ABAQUS is not applied directly but rather is realized by adding field variable exhaustion to the material properties in the model so that the material properties follow the field variable changes. The linear increase is allowed until the model calculation does not converge, and the factor of safety of the slope is calculated according to the instability assessment criteria [43], as given by the following:

$$c_m = c/F_r \quad (3)$$

$$\varphi_m = \arctan(\tan \varphi / F_r) \quad (4)$$

where  $F$  is the factor of safety,  $F_r$  is the discount factor and is the discounted strength index obtained by dividing the cohesive force and the angle of internal friction simultaneously by an ever-changing discount factor  $F_r$ .

Field variables were added to the materials in the model to discount their shear strength, and the calculations were rerun to obtain a factor of safety for the slope. From the previous analysis, it is obtained that the maximum displacement area is found at the foot of the excavation surface (i.e., the main distribution area of plastic strain); therefore, this is taken as the horizontal displacement characteristic point. The horizontal displacement at the foot of the slope is plotted versus the change in the reduction factor, and the reduction factor at the time of the inflection point mutation is the safety factor of the slope. The relationship curve between the displacement and discount factor was obtained after finite element calculations, and the safety coefficients of the plain soil slope and improved soil slope under rainfall conditions were found to be 1.06 and 1.42, respectively; the safety coefficient of the improved soil increased by 25.35% compared with that of plain soil. The factor of safety for the vegetative soil is close to 1, indicating that the vegetative soil slopes are about to reach a state of limiting equilibrium after rainfall, whereas the improved soil slopes remain in a stable state after rainfall. The addition of fly ash to granite residual soils is recommended to improve their slope stability.

Liu et al. [24] also studied the use of fly ash to improve granite residual soils. In their study, they showed that the shear strength of granite residual soil was improved and the permeability coefficient was reduced after a sufficient age of maintenance (e.g., 14 days), and the optimum dosage of fly ash was also 15%. They concluded that fly ash can effectively improve the stability of granite residual soils with respect to water, i.e., with the addition of water, the strength of granite residual soils improved by fly ash will be higher than that of plain soils. The numerical simulation results in this chapter show that granite residual soil modified by 15% fly ash is more stable than plain soil after rainwater erosion. This coincides with the results of Liu et al. Therefore, it can be concluded that fly ash can improve the stability of granite residual soil slopes under rainfall conditions, and 15% fly ash is the optimum dosage.

## 5. Conclusions

The following conclusions can be drawn from this paper's analysis of the deformation-mechanical response during triaxial shear tests of granite residual soil and improved soil mixed with fly ash, as well as from the examination of variable head infiltration tests, microstructural observations and finite-element numerical simulations of granite residual soil backfilled slopes:

- (1) Fly ash may be effectively added to granite residual soil to increase its shear strength. There may be an optimal amount of fly ash inclusion because the cohesiveness and internal friction angle of the soil body also first increase and then decrease. The granite residual soil boosted by fly ash had a cohesiveness of 38.51 kPa and an internal friction angle of 22.15° at a dose of 15% fly ash, which are greater than those of the

vegetative soil by 213.6% and 14.12%, respectively. Fly ash primarily strengthens soil cohesiveness, which counteracts the increase in the angle of internal friction to increase the shear strength of granite residual soil. Upon fly ash addition, the permeability coefficient of the granite residual soil dramatically decreased; nevertheless, the permeability coefficients of the granite residual soil with varying quantities of fly ash did not significantly differ from one another. Fly ash effectively increases the durability of residual granite soils against erosion from rainfall.

- (2) Fly ash is used to improve the granite residual soil mechanism because the amount of granite residual soil particles between the gaps is too large, the interaction force between the particles is small and small particles in the fly ash used to fill the gaps can be uniformly distributed in the soil body between the gaps and generate flocculent or mesh structures in the crystalline material to enhance the interaction of the soil particles with the soil body to improve the shear strength of the soil body. The gelling material produced by the interaction of fly ash filling soil pores simultaneously reduces the permeability of the granite residual soil and the pore channels within the soil. Within a limited range, fly ash can be added to the soil to increase its strength; however, once the dose reaches its maximum, the fly ash fills the soil pores entirely. Further fly ash addition will not significantly improve the strength of the granite residual soil; rather, it will erode the skeleton of the soil and decrease its shear strength.
- (3) Under rainfall conditions, the displacement of granite residual soil slopes decreased after the incorporation of fly ash, and the displacement area changed from being concentrated in the fill area to a distribution that extended toward the excavated soil. Compared with those of vegetative soil slopes, plasticity cloud maps of improved soil slopes show a shift from a circular plastic zone running through the slope to the zone that extends toward the interior of the slope with values that are one order of magnitude lower. Under rainfall conditions, the safety factor of the fly ash-containing granite residual soil was much greater than that of regular backfill. This is due to the filling of the soil gaps with fly ash mixed into the granite residual soil. This filling considerably lowers the permeability coefficient and increases the shear strength of the granite residual soil, lowering the possibility that it will disintegrate in the event of rain. To fortify backfilled slopes, it is advised to add the necessary amount of fly ash when backfilling granite residual soil.

**Author Contributions:** Conceptualization, B.H. and Q.H.; methodology, B.H.; writing—original draft, B.H.; resources, G.T.; review and editing, G.T.; funding acquisition, Y.L.; visualization, Y.L. All authors have read and agreed to the published version of the manuscript.

**Funding:** National Natural Science Foundation of China: 52078195; General Program of National Natural Science Foundation of China: U22A20232.

**Institutional Review Board Statement:** Not applicable.

**Informed Consent Statement:** Not applicable.

**Data Availability Statement:** Data will be made available upon request.

**Conflicts of Interest:** The authors declare that there are no conflicts of interest.

## References

1. Wu, N. *A Study on Characteristics and Some Engineering Problems of Granite Residual Soil with Structural Nature*; Nanjing Forestry University: Nanjing, China, 2005.
2. Gao, J.; Pan, J. Influences of a rainfall on the stability of granite residual soil slopes. In *Geosynthetics in Civil and Environmental Engineering: Geosynthetics Asia 2008, Proceedings of the 4th Asian Regional Conference on Geosynthetics in Shanghai, China, 17–20 June 2008*; Li, G., Chen, Y., Tang, X., Eds.; Springer: Berlin/Heidelberg, Germany, 2009; pp. 847–851.
3. Yin, S.; Huang, J.; Li, X.; Bai, L.; Zhang, X.; Li, C. Experimental study on deformation characteristics and pore characteristics variation of granite residual soil. *Sci. Rep.* **2022**, *12*, 12314. [[CrossRef](#)]
4. Rahardjo, H.; Aung, K.K.; Leong, E.C.; Rezaur, R.B. Characteristics of residual soils in Singapore as formed by weathering. *Eng. Geol.* **2004**, *73*, 157–169. [[CrossRef](#)]

5. Coutinho, R.Q.; Silva, M.M.; Santos, A.N.; Lacerda, W.A. Geotechnical characterization and failure mechanism of landslide in granite residual soil. *J. Geotech. Geoenviron. Eng.* **2019**, *145*, 05019004. [[CrossRef](#)]
6. Zheng, M.; Jian, W.; Wu, M. Reliability analysis of stability of granite residual soil slope. *Chin. J. Rock Mech. Eng.* **2005**, *24*, 5337–5340.
7. Liu, X.; Zhang, X.; Kong, L.; Wang, G.; Li, C. Multiscale structural characterizations of anisotropic natural granite residual soil. *Can. Geotech. J.* **2023**, *60*, 1383–1400. [[CrossRef](#)]
8. Gomes, A.T.; Da Fonseca, A.V.; Cardoso, A.S. Soil water characteristic curve for a granite residual soil: Experimental and numerical results. *Defect Diffus. Forum* **2011**, *312–315*, 1172–1177. [[CrossRef](#)]
9. Veylon, G.; Mouali, L.; Benahmed, N.; Peyras, L.; Duriez, J.; Dias, D.; Antoinet, E. A general model for the small-strain stiffness of saturated residual soils: Back analysis of a database and case study. *Eur. J. Environ. Civ. Eng.* **2023**, *1–17*. [[CrossRef](#)]
10. Li, C.; Kong, L.; Shu, R.; An, R.; Zhang, X. Disintegration characteristics in granite residual soil and their relationship with the collapsing gully in South China. *Open Geosci.* **2020**, *12*, 1116–1126. [[CrossRef](#)]
11. Liu, X.; Zhang, X.; Kong, L.; Wang, G.; Lu, J. Disintegration of granite residual soils with varying degrees of weathering. *Eng. Geol.* **2022**, *305*, 106723. [[CrossRef](#)]
12. Liu, W.; Song, X.; Luo, J.; Hu, L. The processes and mechanisms of collapsing erosion for granite residual soil in southern China. *J. Soils Sediments* **2020**, *20*, 992–1002. [[CrossRef](#)]
13. Liu, X.; Zhang, X.; Kong, L.; Wang, G.; Liu, H. Formation mechanism of collapsing gully in southern China and the relationship with granite residual soil: A geotechnical perspective. *Catena* **2022**, *210*, 105890. [[CrossRef](#)]
14. Deng, X.; He, Z.M.; Fu, H.Y.; Zeng, L. Impact of rainfall infiltration on slope stability of high embankment with granite residual soil. *Min. Metall. Eng.* **2016**, *36*, 11–15.
15. Zhang, L.; Peng, X.; Zheng, B.; Liu, Y. Study on mechanics properties and improvement mechanism of lime improved granite residual soil. *Highw. Eng.* **2019**, *44*, 271–276.
16. Luo, X.; Fu, M. Experimental study on strength and deformation of unsaturated soil of lime treatment. *Yangtze River* **2017**, *48*, 86–90.
17. Li, Z.; Chen, Z.; Hu, P.; An, Y. Study on strength characteristics of lignin-treated granite residual soil. *Res. Explor. Lab.* **2019**, *38*, 30–33+55.
18. Li, Z.; Chen, Z.; Hu, P.; An, Y. Compression characteristics of flyash-lime treated granite residual soil. *J. Water Resour. Archit. Eng.* **2019**, *17*, 82–86.
19. Sun, Y.; Liu, Q.; Xu, H.; Wang, Y.; Tang, L. Influences of different modifiers on the disintegration of improved granite residual soil under wet and dry cycles. *Int. J. Min. Sci. Technol.* **2022**, *32*, 831–845. [[CrossRef](#)]
20. Chang, A.C.; Lund, L.J.; Page, A.L.; Warneke, J.E. Physical properties of fly ash-amended soils. *J. Environ. Qual.* **1977**, *6*, 267–270. [[CrossRef](#)]
21. Moussadik, A.; El Fadili, H.; Saadi, M.; Diouri, A. Lightweight aerated concrete based on activated powders of coal gangue and fly ash. *Constr. Build. Mater.* **2024**, *417*, 135333. [[CrossRef](#)]
22. Pathan, S.M.; Aylmore, L.A.G.; Colmer, T.D. Properties of several fly ash materials in relation to use as soil amendments. *J. Environ. Qual.* **2003**, *32*, 687–693. [[CrossRef](#)]
23. Li, L.-H.; Yu, C.-D.; Hu, Z.; Liu, Y.-M.; Zhang, J.; Li, J.-P. Large-scale triaxial tests on reinforced fly ash and sand mixture. *J. Yangtze River Sci. Res. Inst.* **2019**, *36*, 97–103+111.
24. Liu, S.; Chen, Z.; Chen, W.; Wei, Y. Experience study on granite residual soil improved by fly ash. *J. Fuzhou Univ. (Nat. Sci. Ed.)* **2018**, *46*, 712–717.
25. Xie, B.; Zhang, W.; Zhang, B.; Ji, G.; Cui, J. Experimental study on unconsolidated and undrained shear strength of fly ash cement soil at different ages. *J. Eng. Geol.* **2021**, *29*, 1216–1223.
26. Wang, Z.; Zheng, C.; Zhang, L.; Xiong, K.; Li, Z. Research progress on stability analysis methods of granite residual soil slope. *E3S Web Conf.* **2023**, *375*, 01056. [[CrossRef](#)]
27. Li, S.; Niu, Y.; Wang, B.; Gao, Y.; Zhu, Y. Influence of rainfall infiltration on stability of granite residual soil high slope. *Math. Probl. Eng.* **2022**, *2022*, 1920403. [[CrossRef](#)]
28. Xu, X.; Jian, W.; Wu, N.; Xu, X. Modeltest of rainfall-induced residual soil slope failure. *China J. Highw. Transp.* **2018**, *31*, 270–279.
29. Hu, H.; Wu, X.; Zhang, Y. Failure mode analysis of granite residual soil slope based on rainfall land slide simulation test. *J. Xiamen Univ. (Nat. Sci.)* **2021**, *60*, 1098–1102.
30. Guo, Y.; Li, S.; Zhang, J.; Wang, B.; Gao, Y. Study on the seepage mechanism of rainwater on granite residual soil cut slopes. *Adv. Civ. Eng.* **2023**, *2023*, 1259527. [[CrossRef](#)]
31. Chen, J.; Lei, X.-W.; Zhang, H.-L.; Lin, Z.; Wang, H.; Hu, W. Laboratory model test study of the hydrological effect on granite residual soil slopes considering different vegetation types. *Sci. Rep.* **2021**, *11*, 14668. [[CrossRef](#)]
32. Xu, J.; Ni, Y. Prediction of grey-catastrophe destabilization time of a granite residual soil slope under rainfall. *Bull. Eng. Geol. Environ.* **2019**, *78*, 5687–5693. [[CrossRef](#)]
33. Liu, W.; Ouyang, G.; Luo, X.; Luo, J.; Hu, L.; Fu, M. Moisture content, pore-water pressure and wetting front in granite residual soil during collapsing erosion with varying slope angle. *Geomorphology* **2020**, *362*, 107210. [[CrossRef](#)]
34. Yang, H.Q.; Zhang, L. Bayesian back analysis of unsaturated hydraulic parameters for rainfall-induced slope failure: A review. *Earth-Sci. Rev.* **2024**, *251*, 104714. [[CrossRef](#)]
35. Liu, W.; Cui, Y.; Ouyang, G.; Lyu, Z. An experimental study on influence of grain-size composition on collapsing erosion of granite residual soil. *Catena* **2023**, *223*, 106949. [[CrossRef](#)]
36. Ismail, K.N.; Hussin, K.; Idris, M.S. Physical, chemical and mineralogical properties of fly ash. *J. Nucl. Relat. Technol.* **2007**, *4*, 47–51.

37. Zhao, Y.; Zhang, J.; Tian, C.; Li, H.; Shao, X.; Zheng, C. Mineralogy and chemical composition of high-calcium fly ashes and density fractions from a coal-fired power plant in China. *Energy Fuels* **2010**, *24*, 834–843. [[CrossRef](#)]
38. Zhang, W.; Xie, J.; Liu, D.; Wang, S. Study on mechanical properties of peat soil improved by cement and high calcium fly ash. *J. Henan Polytech. Univ. (Nat. Sci.)* **2020**, *39*, 161–167.
39. Fei, L.-L.; Qian, J.-S. In-situ characteristics of moisture for granite residual soil slope. *J. Highw. Transp. Res. Dev.* **2020**, *37*, 29–35.
40. Zhang, L. *Stability Analysis of Expansive Soil Slope with Rainfall Infiltration*; China University of Geosciences: Beijing, China, 2016.
41. Yang, L.-L.; Fang, X.-Q.; Yuan, L.; Guo, X.-M.; Cao, Y.; Zhang, X.-X.; Chen, Y.-H. Flash flood factors sensitivity analysis and disaster risk assessment in Jiangxi province. *Sci. Technol. Eng.* **2023**, *23*, 4448–4456.
42. Zheng, Y.; Zhao, S. Application of strength reduction fem in soil and rock slope. *Chin. J. Rock Mech. Eng.* **2004**, *23*, 3381–3388.
43. He, L.; Qian, J.; Zhao, C.; Li, Z. Study on stability analysis method of high fill slope of Wushan Shennv Peak Airport. *J. Hefei Univ. Technol. (Nat. Sci.)* **2023**, *46*, 646–651+703.

**Disclaimer/Publisher’s Note:** The statements, opinions and data contained in all publications are solely those of the individual author(s) and contributor(s) and not of MDPI and/or the editor(s). MDPI and/or the editor(s) disclaim responsibility for any injury to people or property resulting from any ideas, methods, instructions or products referred to in the content.